eprints@whiterose.ac.uk
https://eprints.whiterose.ac.uk/

Self-learning Direct Flux Vector Control of Interior Permanent Magnet Machine Drives

Tianfu Sun, Student Member, IEEE, Jiabin Wang, Senior Member, IEEE, and Mikail Koc, Student Member, IEEE

Abstract—**This paper proposes a novel self-learning control scheme for interior permanent magnet synchronous machine (IPMSM) drives to achieve maximum torque per ampere (MTPA) operation in constant torque region and voltage constraint maximum torque per ampere (VCMTPA) operation in field weakening region. The proposed self-learning control scheme (SLC) is based on the newly reported virtual signal injection aided direct flux vector control. However, other searching based optimal control schemes in the flux-torque (f-t) reference frame are also possible. Initially the reference flux amplitudes for MTPA operations are tracked by virtual signal injection and the data are used by the proposed self-learning control scheme to train the reference flux map online. After training, the proposed control scheme generates the optimal reference flux amplitude with fast dynamic response. The proposed control scheme can achieve MTPA or VCMTPA control fast and accurately without accurate prior knowledge of machine parameters and can adapt to machine parameter changes during operation. The proposed control scheme is verified by experiments under various operation conditions on a prototype 10 kW IPMSM drive.**

Index Terms—**Maximum torque per Ampere (MTPA) operation, Permanent magnet synchronous machine (IPMSM), Self-learning control, Signal injection.**

I. INTRODUCTION

Interior permanent magnet synchronous machines (IPMSM) have many attractive advantages such as high efficiency, high power/torque density, high reliability and good field-weakening performance [1]. In order to control IPMSM operating at the optimal efficiency points, the maximum torque per ampere (MTPA) control [2]–[4] and voltage constrained maximum torque per ampere (VCMTPA) control [5] are proposed in constant torque and field weakening regions, respectively. In literature, to control the IPMSM, either field oriented control in the rotor synchronous (d-q) frame [3], [6] or direct torque control or direct flux vector control [7] in the flux linkage synchronous (f-t) frame [8]–[10] are proposed. Compared with the d-q frame based control, the f-t frame based control can regulate the stator flux amplitude directly and can manage motor voltage in field weakening region without look-up tables of current or flux references. Therefore, the f-t frame based control scheme can easily cope with voltage

saturation and have better performance in field weakening region [11].

Currently, MTPA operations for f-t frame based control schemes are mainly achieved by controlling the reference flux amplitude. The optimal reference flux amplitude can be generated through mathematical model [12] or pre-defined look-up tables which are obtained from experiments or numerical machine model [13]. However, the f-t frame based MTPA control schemes are affected not only by the errors in the reference flux amplitude due to the machine parameter uncertainty and nonlinearity [6], but also by the flux observer errors in the flux control loop [14]. Thus, compared with d-q frame based MTPA control schemes, f-t frame based control schemes are vulnerable to flux errors in the reference and observer [5].

In order to reduce the dependency on motor parameters for MTPA operations with the f-t frame based control of IPMSM drives, a search algorithm was, therefore, proposed in [15]. Although this scheme does not depend on the knowledge of machine parameters, its accuracy was affected by voltage and current harmonics and load torque disturbance. In [16], a signal injection based MTPA point tracking scheme was proposed based on the principle of extremum seeking control (ESC) [17], [18]. The MTPA tracking is based on the fact that the rate of change of current amplitude with respect to injected reference flux perturbation at MTPA points is zero. Instead of injecting sinusoidal signal at fixed frequency [18]–[20], this control method injects a random signal into the reference flux amplitude to avoid the residual torque harmonic at the injected signal frequency. However, as a result of the injected signal, this method causes additional copper/iron loss and additional torque ripple. Moreover, the errors in flux observer may also deteriorate the MTPA control quality.

To address the problems associate with the f-t frame based control methods described previously, a novel concept that utilizes d-q frame based searching techniques to compensate the MTPA control errors of the f-t frame based control schemes was proposed in [14]. This control scheme utilizes the virtual signal injection to track the MTPA points in the f-t frame and is robust to flux observer error and motor parameters inaccuracy in tracking MTPA points. Since this control scheme does not inject real signals into the motor drive, it will not cause additional iron loss and copper loss. However, this control scheme also suffers from the slow converging rate and poor dynamic performance.

In order to improve the converging rate and dynamic performance, a self-learning control scheme based on virtual signal injection was proposed in the d-q frame [21]. Since the

virtual signal injection can track the MTPA points accurately, this control scheme uses the tracked MTPA points to establish the relationship between the optimal d-axis current and torque command through on-line training. After training, the control scheme generates the optimal reference d-axis current with fast response. However, in the field weakening region, the optimal d-axis current is dependent on both torque and rotor speed. Therefore, this control scheme will no longer be effective in the field weakening region.

In this paper, self-learning control for IPMSM drives is proposed based on virtual signal injection based direct flux vector control in the f-t frame. The proposed control scheme achieves MTPA operation through on-line learning in constant torque region and directly limits stator flux amplitude for VCMTPA operation in field weakening. In this way, the proposed control scheme not only has the advantages of virtual signal injection aided direct flux vector control such as insensitive to machine parameter inaccuracy, robust to current and voltage harmonics, high accuracy in tracking the MTPA and VCMTPA points, and no additional iron and copper losses, but also has fast dynamic responses in both constant torque and field weakening regions and can adapt to machine parameter changes automatically.

II. Principle of Proposed Control Scheme

A. Mathematical Model of IPMSM in f-t Frame

The relationship between the flux linkage synchronous (f-t) reference frame and the classic (d-q) frame is illustrated in Fig. 1. In the f-t frame, the f-axis is aligned with the stator flux vector while the t-axis leads the f-axis by 90 degrees. The angular displacements of the f-axis with respected to the d-axis and the stationary α-axis are δ and $\theta_e + \delta$, respectively, where θ_e is the angular displacement between the d-axis and the α-axis.

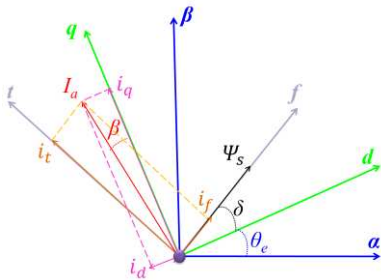Fig. 1. α-β reference frame, f-t reference frame and d-q reference frame.

For the f-t frame based control scheme, the flux amplitude can be controlled or limited directly. The mathematical model of an IPMSM in the f-t frame can be expressed in (1) to (6). v_f and v_t are the f- and t-axis voltages, i_f, i_t are the f- and t-axis currents, R is the stator phase resistance, T_e is the electromagnetic torque, p is the number of pole pairs, Ψ_s is the stator flux amplitude and ω_m is the rotor angular speed. I_{lim} and v_{lim} are the maximum current amplitude and voltage amplitude, respectively. The direct flux vector control scheme [14] can be achieved by controlling the i_t and Ψ_s under the condition that the stator flux vector is estimated by a flux observer.

$$v_f = Ri_f + \frac{d\Psi_s}{dt} \tag{1}$$

$$v_t = Ri_t + \Psi_s\left(p\omega_m + \frac{d\delta}{dt}\right) \tag{2}$$

$$T_e = \frac{3}{2}p\Psi_s i_t \tag{3}$$

$$\sqrt{I_{lim}^2 - I_f^2} \geq i_t \tag{4}$$

$$\frac{3}{2}p\Psi_s\sqrt{I_{lim}^2 - I_f^2} \geq T_e \tag{5}$$

$$\frac{1}{p\omega_m}\left[\sqrt{v_{lim}^2 - \left(Ri_f\right)^2} - Ri_t\right] \geq \Psi_s \tag{6}$$

B. Relationship Between Optimal Stator Flux Amplitude and Torque

For a given torque command, in constant torque region, there is a unique optimal stator flux amplitude for the MTPA operation [14]. The relationship between torque command and the optimal stator flux for MTPA operation is shown in Fig. 2. If a sufficient number of MTPA points are tracked online, other points on the curve can be approximated by interpolations among these tracked points. The proposed self-learning control scheme is based on this simple but effective concept.
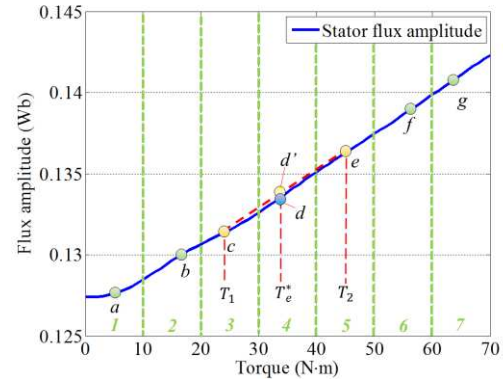

Fig. 2. Relationship between torque command and the optimal stator flux for MTPA operation based on machine parameters in Table I. The point d is the optimal flux amplitude corresponding to T_e^* and the point d' is the interpolated flux amplitude based on points c and e, which will be detailed in Section III.

When the motor drive is operating in the field weakening region, the stator voltage is constrained by the maximum voltage. Fig. 3 shows the variations of torque and voltage amplitudes with stator flux amplitude for a given current amplitude when the required voltage for the MTPA operation is larger than the voltage limit. The derivative of torque with respect to the current angle, $\partial T_e/\partial\beta$, is also shown in Fig. 3. The current angle, β, is the angle between the q-axis and the current vector as shown in Fig. 1. As the flux amplitude increases towards the MTPA point, the resultant torque and voltage amplitude, v_a^*, will increase. Therefore, the voltage constrained maximum torque per ampere (VCMTPA) operation point is the point at which the voltage amplitude is equal to the voltage limit [5]. At the VCMTPA point, the maximum torque at the intersection is achieved for the given current amplitude and voltage limit.
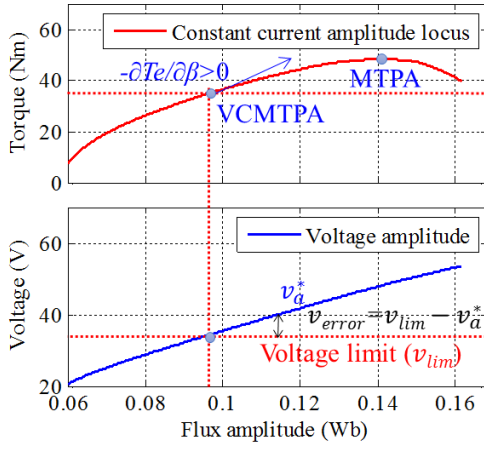
Fig. 3. Torque and voltage amplitude variations with flux amplitude for given current amplitude.

According to (6), the maximum flux amplitude under the voltage constraint is parameter-independent except for the phase resistance. However, the voltage drop across the resistance is relatively small compared with the voltage limit. Therefore, by assuming the nominal value of the phase resistance at a representative temperature, the optimal flux amplitude for VCMTPA operations can be obtained by (6) directly.

III.   IMPLEMENTATION OF THE PROPOSED SELF-LEARNING CONTROL SCHEME

The proposed self-learning control scheme is based on virtual signal injection aided direct flux vector control, albeit
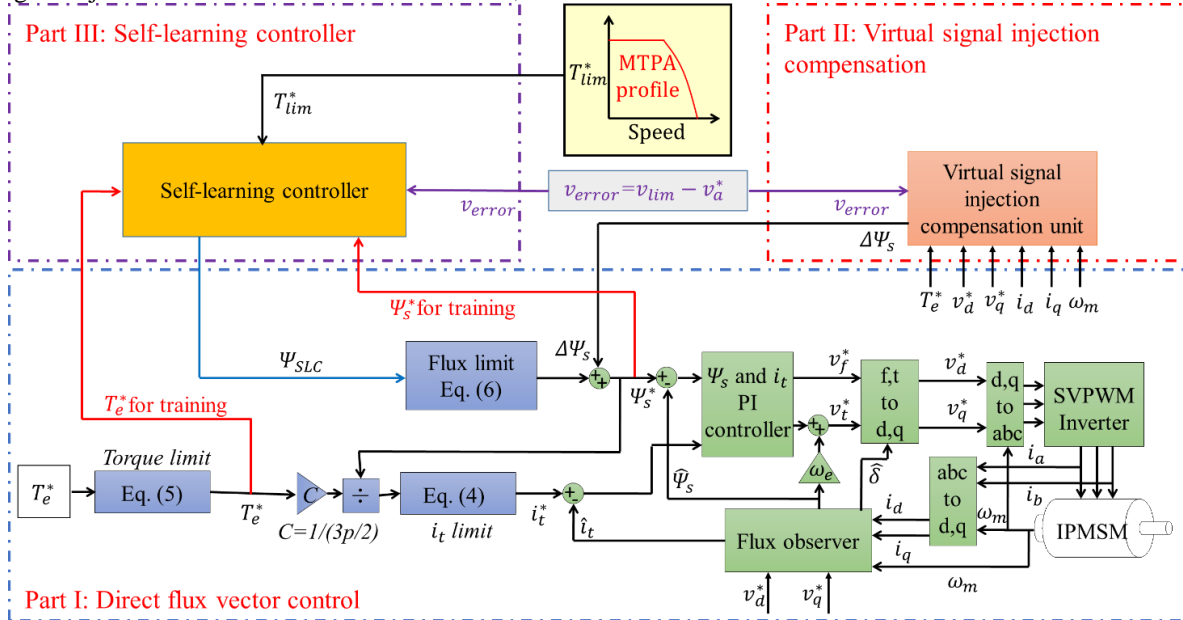
other searching based optimal control schemes in the f-t frame is also possible. The virtual signal injection aided direct flux vector control combines the direct flux vector control scheme [7] and the virtual signal injection compensation [14]. The direct flux vector control can limit the current amplitude in the f-t frame and easily cope with the voltage limit, and hence has better performance in the field weakening region [7]. Moreover, the virtual signal injection compensation is parameter insensitive and robust to flux observer error [14]. Therefore, the virtual signal injection aided direct flux vector control inherently has the advantages of both the direct flux vector control and virtual signal injection compensation.

A.   Direct Flux Vector Control

The schematic of the direct flux vector control scheme is shown in part I of Fig. 4 and more details can be found in [7], [22], [23]. The reference flux amplitude, Ψ_{SLC}, is generated from the proposed self-learning control scheme which will be described in part C of this section. The output of the self-learning control scheme is limited by (6) to ensure the IPMSM drive operates within the voltage limit. The reference torque is limited by (5). The t-axis current is calculated by (3) and limited by (4) to ensure the IPMSM drive operates within the current limit. As proposed in [7], the stator flux linkage is directly regulated by the f-axis voltage and the t-axis current is regulated by the t-axis voltage through two PI controllers. The flux observer in this paper is the conventional flux observer described in [14] and [24]. However, other observers are also applicable.

Fig. 4. Schematic of the proposed control scheme.

B.   Virtual Signal Injection Compensation Unit

In order to generate optimal reference flux amplitude before the self-learning controller is trained, the self-learning control output, Ψ_{SLC}, is conditioned by the virtual signal injection compensation as shown in Part II of Fig. 4. The details of the

compensation unit are shown in Fig. 5. The inputs of the virtual signal injection compensation unit are the d- and q-axis reference voltage (v_d^*, v_q^*), the measured d- and q-axis currents (i_d, i_q), the measured rotor speed (ω_m) and the voltage error (v_{error}) given in (7).

$$v_{error} = v_{lim} - v_a^* \tag{7}$$

where v_a^* is the amplitude of the generated reference voltage and v_{lim} is the maximum achievable voltage amplitude. The output of the virtual signal injection compensation unit is the reference flux amplitude error compensation term ($\Delta\Psi_s$). ΔT_e^* and ε in Fig. 5 are the change in the reference torque and a pre-defined threshold, respectively, which will be discussed in part C of this section.
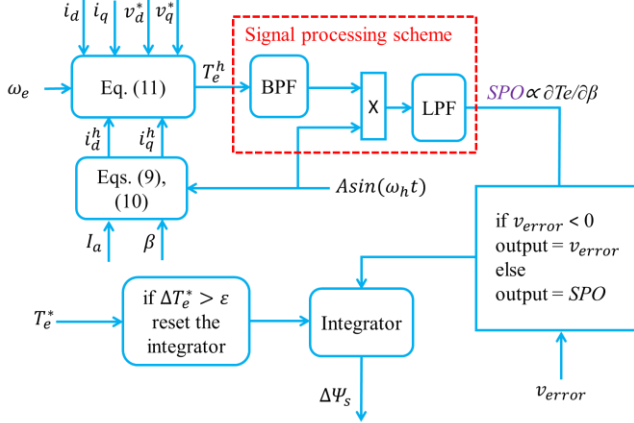

Fig. 5. Details of the virtual signal injection compensation unit.

As described in [5], [6], a high frequency signal, $\Delta\beta$, is injected into the current angle through the mathematical expressions in (8) to (10) where ω_h is the angular frequency of the injected signal. In order to minimize the influences of the fundamental component and other harmonics on the output of the virtual signal injection, the frequency of the injected signal should be as high as possible but the maximum frequency is limited by the sample rate of the controller. In this study, the injected signal frequency is 1 kHz.

$$\Delta\beta = A sin(\omega_h t) \tag{8}$$
$$i_d^h = -I_a sin(\beta + \Delta\beta) \tag{9}$$
$$i_q^h = I_a cos(\beta + \Delta\beta) \tag{10}$$

The resultant torque with high frequency component, T_e^h, can be calculated by (11) [6]. It is worth noting that T_e^h is obtained from the mathematical calculations and no real signal is injected into the motor current angle, therefore, this method is termed as virtual signal injection.

$$T_e^h(\beta + \Delta\beta) = \frac{3}{2}\left[\frac{(v_q^* - Ri_q)}{\omega_m} + \frac{(v_q^* - Ri_d)}{i_q\omega_m}i_d^h\right]i_q^h \tag{11}$$

Based on Taylor's series expansion, the left hand side of (11) can be expressed as (12).

$$T_e^h(\beta + \Delta\beta) = T_e^h(\beta) + \frac{\partial T_e^h}{\partial\beta}A sin(\omega_h t)$$
$$+ \frac{1}{2}\frac{\partial}{\partial\beta}\left(\frac{\partial T_e^h}{\partial\beta}\right)A^2 sin^2(\omega_h t) + \cdots \tag{12}$$

As shown in Fig. 5, the 1st, 3rd and other higher order terms in (12) are removed by the band-pass filter (BPF) whose center frequency is equal to ω_h. The output of the BPF is further multiplied by $sin(\omega_h t)$ and the result will contain a constant component which is proportional to $\partial T_e/\partial\beta$ as shown in (13).

$$m\frac{\partial T_e}{\partial\beta}A sin^2(\omega_h t) = \frac{1}{2}mA\frac{\partial T_e}{\partial\beta} - \frac{\partial T_e}{\partial\beta}mA cos(2\omega_h t) \tag{13}$$

The low-pass filter (LPF) in Fig. 5 will eliminate the high frequency term in (13) and its output, SPO, will be proportional to $\partial T_e/\partial\beta$. This signal is used by the PI controller in Fig. 5 to adjust the reference flux compensation term, $\Delta\Psi_s$, until $\partial T_e/\partial\beta = 0$, i.e., the MTPA point is tracked. Since $\partial T_e/\partial\beta$ should be equal to zero at the MTPA point, SPO signal can be defined as a MTPA quality indicator. Since (11) is based on the command voltages and measured currents in the d-q reference frame, the flux observer error will not affect the accuracy of the MTPA tracking performance. Indeed, the error between the optimal flux amplitude and the reference flux amplitude will be compensated by the output of the virtual signal injection compensation unit, $\Delta\Psi_s$, shown in Fig. 5. The details about the effects of flux observer error on the virtual signal injection were discussed in [14].

In field weakening region, the voltage limit will be reached before $\partial T_e/\partial\beta = 0$. Thus, the virtual signal injection should be suspended in the field weakening region and the stator flux amplitude should be limited by (6). However, due to voltage drop in the inverter, phase resistance deviation from the nominal value and flux observer error, the voltage saturation may still occur. To avoid the voltage saturation, the voltage error, v_{error}, is fed to the PI controller instead of SPO to reduce $\Delta\Psi_s$ when v_{error} is negative, i.e., when the amplitude of the inverter reference voltage is greater than the voltage limit.

The sign of v_{error} determines whether SPO or v_{error} is fed to the PI controller. If $v_{error} \geqslant 0$, the drive voltage amplitude is below the voltage limit, the signal SPO will be fed to the integrator controller in Fig. 5 to adjust $\Delta\Psi_s$ until the MTPA point is reached or the voltage amplitude equals to v_{lim}, i.e., the VCMTPA point shown in Fig. 3 is reached. If $v_{error} < 0$, v_{error} will be fed to the integrator controller and $\Delta\Psi_s$ will decrease until $v_{error} = 0$, i.e., the VCMTPA point is realized. Therefore, the virtual signal injection aided direct torque control can always guarantee that the motor is operating on the MTPA or VCMTPA point.

C. Self-learning Controller

In order to generate accurate optimal reference flux amplitudes for MTPA and VCMTPA control with fast response, the proposed self-learning control scheme utilizes curve fitting to approximate the relationship between reference torque and optimal flux amplitude in constant torque region and utilizes (6) to limit flux amplitude in field weakening region. The details of the proposed control scheme will be illustrated below.

1) In constant torque region

As shown in Fig. 4, the inputs of the self-learning controller include the voltage error, v_{error}, the reference stator flux amplitude, Ψ_s^*, the limited reference torque, T_e^* and the maximum reference torque of MTPA operation for a given speed, T_{lim}^*. The outputs of the self-learning controller is denoted as Ψ_{SLC}. Any error in Ψ_{SLC} due to curve fitting or imperfect learning will be compensated by $\Delta\Psi_s$ to generate an accurate flux amplitude reference Ψ_s^* for MTPA or VCMTPA operation as described previously. Fig. 2 shows the relationship between optimal flux amplitude and corresponding reference torque in constant torque region. If a sufficient number of MTPA points, e.g., a to g in Fig. 2, are recorded, other points on the curve can be approximated by interpolations among these

recorded points. These optimal flux amplitude and corresponding torque command are recorded in the two column vectors $\mathbf{\Psi}_{sMTPA}$ and $\mathbf{T}_{MTPA}$, respectively. In order to have an even distribution of the recorded MTPA points over the applicable torque range, the torque command range is divided into N sections and each section records one tracked MTPA point. For example, the torque command region in Fig. 2 is divided into seven sections. If a new pair of optimal flux amplitude and torque command for MTPA operation is tracked in section M, the Mth elements of $\mathbf{\Psi}_{sMTPA}$ and $\mathbf{T}_{MTPA}$ will be substituted by the corresponding values of the newly tracked MTPA point. This

process repeats during the self-learning operation. In this way the proposed control scheme can always adapt itself to machine parameter variations during operation.

The schematic of the proposed self-learning control is shown in Fig. 4 and the flow chart of the self-learning control algorithm for MTPA operation is shown in Fig. 6. Two column vectors $\mathbf{\Psi}_{sMTPA}$ and $\mathbf{T}_{MTPA}$ record the tracked stator flux amplitude, Ψ_s^*, and the corresponding torque reference, T_e^*, respectively. μ is a pre-defined threshold to determine whether $\mathbf{\Psi}_{sMTPA}$ and $\mathbf{T}_{MTPA}$ should be updated or not.
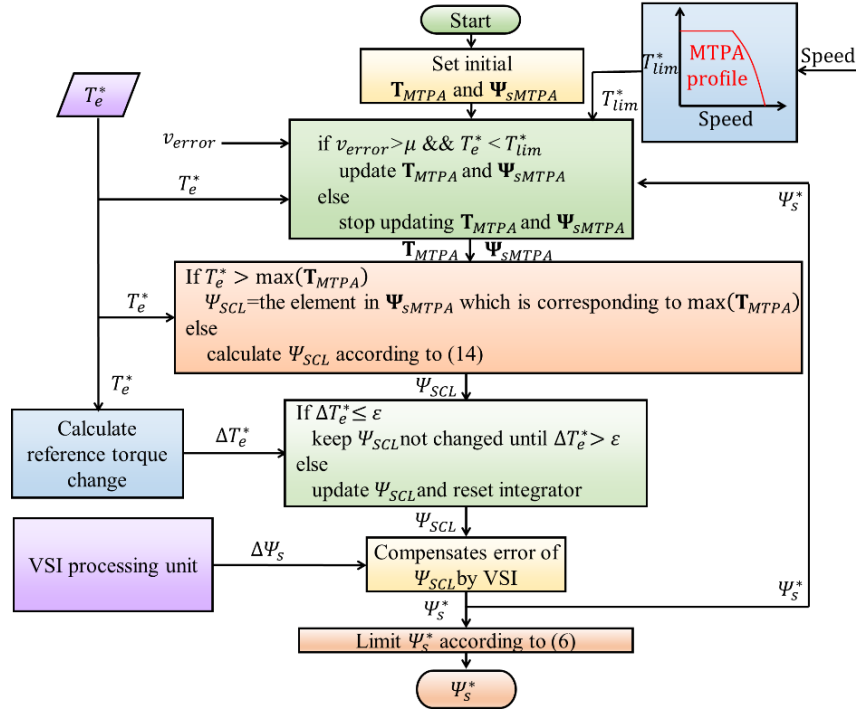

Fig. 6. Flow chart of self-learning control algorithm.

Before training, $\mathbf{\Psi}_{sMTPA}$ and $\mathbf{T}_{MTPA}$ may be assigned with nominal values or data for MTPA operation generated off-line. If a torque demand, T_e^*, is located between two elements of $\mathbf{T}_{MTPA}$, e.g., T_1 and T_2 in Fig. 2, the corresponding MTPA point d can be approximated by d' through (14). The error between Ψ_{SLC} and Ψ_s^* can be compensated by $\Delta\Psi_s$.

$$\Psi_{SLC} = \frac{T_e^* - T_2}{T_1 - T_2}(\Psi_1 - \Psi_2) + \Psi_2 \qquad (14)$$

If T_e^* is larger than any recorded torque reference in $\mathbf{T}_{MTPA}$, the output of the proposed self-learning control scheme will be equal to the element in $\mathbf{\Psi}_{sMTPA}$ which corresponds to the reference flux amplitude associated with the maximum torque reference in $\mathbf{T}_{MTPA}$, i.e., Max($\mathbf{T}_{MTPA}$). The error between Ψ_{SLC} and optimal Ψ_s^* can also be compensated by $\Delta\Psi_s$.

The output of the integrator in Fig. 5 will have an accumulative value of $\Delta\Psi_s$ that compensates the optimal reference flux error for a given torque. When the absolute value of the torque step, ΔT_e^*, is larger than a pre-defined threshold, ε, the integrator will be reset. This is to ensure the integrator can adjust itself more quickly against the new torque reference. Meanwhile, Ψ_{SLC} will update according to the new reference torque based on the data recorded in $\mathbf{T}_{MTPA}$ and $\mathbf{\Psi}_{sMTPA}$ at the

same time when the integrator is reset. When the torque step is smaller than the threshold, because the corresponding change in the reference flux amplitude should be small too, Ψ_{SLC} will not update and the small error will be compensated by the virtual signal injection in short time. In both conditions $\mathbf{T}_{MTPA}$ and $\mathbf{\Psi}_{sMTPA}$ will be updated continuously by the reference torque and resultant reference flux amplitude.

When a torque step is larger than the threshold ε, SPO signal will be masked for a small period of time, e.g., 3 times of the t-axis current loop time constant. After SPO is masked, virtual signal injection will drive the resultant reference flux amplitude toward the MTPA point, while $\mathbf{T}_{MTPA}$ and $\mathbf{\Psi}_{sMTPA}$ will be updated continuously by the reference torque and resultant reference flux amplitude. Due to virtual signal injection tends to drive the reference flux amplitude towards the MTPA points, the newly recorded reference flux amplitude in $\mathbf{\Psi}_{sMTPA}$ should be closer to the actual MTPA point than the one which is previously recorded in $\mathbf{\Psi}_{sMTPA}$. Therefore, the accuracy of the SLC output will continuously increase. Moreover, a more accurate SLC output will also accelerate the convergent speed of the reference flux amplitude to the actual MTPA point. Therefore, although the reference flux amplitudes recorded in $\mathbf{\Psi}_{sMTPA}$ may initially have large errors, they will eventually

approximate the ideal MTPA flux amplitudes. Consequently, the proposed SLC can be trained on-line, and the training of the SLC will not affect the MTPA operation.

2) In field weakening region

Since the flux amplitude for the field weakening control is not only dependent on reference torque but also on speed, therefore, the curve fitting based self-learning is not effective in the field weakening region. Thus, the online training of the self-learning control scheme should be suspended in the field weakening region when v_{error} is smaller than a pre-defined threshold μ or if the motor speed and reference torque exceed a pre-defined region, i.e., when $T_e^* \geq T_{lim}^*$, where T_{lim}^* is the maximum torque at a given speed as shown in Fig. 4. In order to achieve accurate VCMTPA operation in the field weakening region with fast response, the reference flux amplitude is limited by (6) directly and it is independent of machine parameters except for stator resistant R. The error between the flux amplitude generated from (6) and the optimal flux amplitude for VCMTPA operation is also compensated by $\Delta\Psi_s$.

IV. SIMULATION RESULTS

Simulations of the self-learning control for both MTPA operation and VCMTPA operation have been performed based on a high-fidelity IPMSM model which accounts all non-linear effects and high order spatial harmonics as described in [25]. The machine specifications are listed in Table I. The motor is controlled in torque control mode in simulations. The applicable reference torque range of the machine is divided into 35 sections, i.e., N=35. The threshold, μ, to suspend the online training of the self-learning control scheme is set to 2V. The threshold of torque step, ε, is set to 2 N·m. Before training, $\mathbf{T}_{MTPA}$ is set to a zero vector and all elements in $\mathbf{\Psi}_{sMTPA}$ are set to the nominal value of 0.1Wb.

TABLE I
IPMSM PARAMETERS

Number of pole-pairs	3
Phase resistance	51.2 mΩ
Continuous/Maximum current	58.5/118 A
Peak power at base speed	10 kW
DC link voltage	120 V
Base/maximum speed	1350/4500 r/min
Continuous/peak torque	35.5/70 Nm
Peak power at maximum speed	7 kW

A. Reference Torque Fast Changes

Simulations were performed for the operating conditions when reference torque changed rapidly. As shown in Fig. 7, the reference torque steps between 20 N·m and 40 N·m in every second ($\Delta T_e^* > \varepsilon$). Before the proposed control scheme is fully trained, i.e., t<6 s, $\Delta\Psi_s$ compensates the error of Ψ_{SLC} and the corresponding reference torque and reference flux amplitude are recorded in $\mathbf{T}_{MTPA}$ and $\mathbf{\Psi}_{MTPA}$, respectively. At each torque step, the integrator is reset meanwhile the SLC output is updated based on the data recorded in $\mathbf{T}_{MTPA}$ and $\mathbf{\Psi}_{MTPA}$, simultaneously. As it can be seen in Fig. 7, the accuracy of the SLC output continuously increases and the SLC outputs eventually equal to the optimal values. After training, i.e., when t > 6 s, the proposed control scheme can instantly generate an accurate optimal reference flux amplitude for a given torque demand.
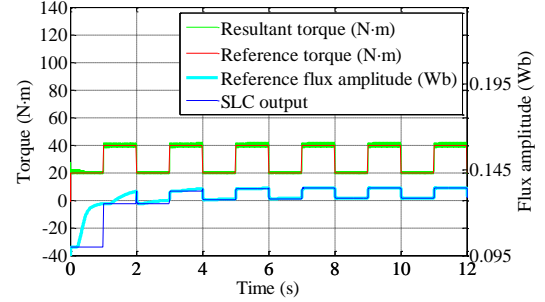

Fig. 7. Responses of torque and stator flux amplitude to rapid reference torque changes.

B. Reference Torque Step Smaller Than the Threshold

Fig. 8 shows the simulation results when the reference torque step is smaller than the threshold, ε. As shown in Fig. 8, when t<35 s, the proposed control scheme is not trained, the reference torque slowly increased with a 2 N·m/s gradient. Under this condition, the integrator in Fig. 8 will not be reset and Ψ_{SLC} will not update. The reference flux amplitude is generated from the combination of Ψ_{SLC} and $\Delta\Psi_s$. However, the proposed control scheme is still under training during the process. When t>35 s, the SLC generates the optimal reference flux amplitude directly with fast response.
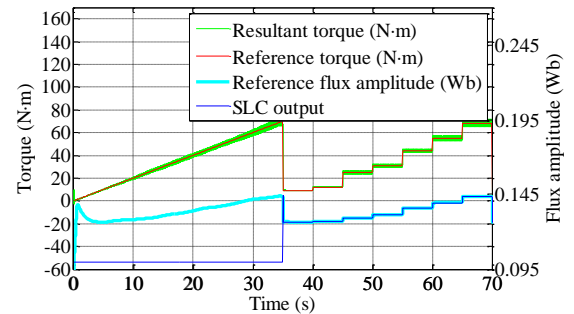

Fig. 8. Responses of reference flux amplitude and SLC outputs when reference torque changes slowly.

C. Automatic Adaptation to Machine Parameter Change

The adaptation of the proposed SLC to significant PM flux change is also investigated by simulation. As shown in Fig. 9, at t=70 s, the permanent magnet (PM) flux linkage in the machine model is reduced to 80 percent of its original value while the parameter in the flux observer is not changed. This may represent the combined effect of temperature increase and partial demagnetization of the machine. The change in the PM flux linkage causes the new MTPA points to deviate from the original MTPA points and the differences are compensated by the virtual signal injection. Meanwhile $\mathbf{T}_{MTPA}$ and $\mathbf{\Psi}_{sMTPA}$ are updated according to newly tracked MTPA points continuously. It can be seen from Fig. 9 that in the first cycle after the parameter change when 70s≤ t ≤105s, the reference flux amplitude is obtained from the sum of the SLC output and $\Delta\Psi_s$ and changes slowly in response to the torque changes while the overshoots of the reference flux amplitude can also be observed. During this period, the proposed SLC is trained by the newly tracked MTPA reference flux amplitude.

In the second cycle after the machine parameter change when t >105s, the proposed SLC has adapted itself to the new machine parameter and the outputs of the SLC quickly converge the new MTPA reference flux amplitudes. The training of the SLC does not affect MTPA operations of the IPMSM drive, albeit the torque control error increases due to the inaccurate machine parameter in the flux observer. However, if the flux observer is machine parameter independent, such as voltage model based flux observer with ideal inverter voltage drop compensation, the torque error can be reduced.
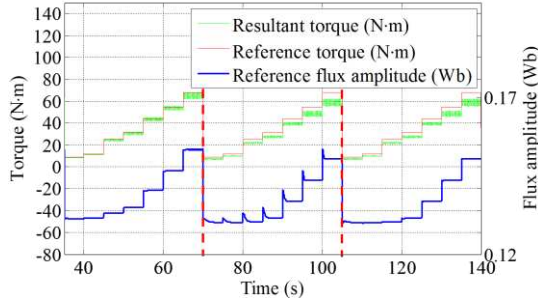

Fig. 9. Responses of reference torque, reference flux amplitude and resultant torque before and after PM flux linkage change at 1000 r/min.

D. Transition Between Constant Torque Region and Field Weakening Region

The performances of the proposed control scheme, when operation conditions change between the constant torque region and field weakening region, were also simulated. As shown in Fig. 10, the reference torque varies between 9 N·m and 68 N·m in steps, periodically. When t <35s, the proposed control scheme has not been fully trained, the reference flux amplitude is generated from the combination of Ψ_{SLC} and $\Delta\Psi_s$ and converge gradually to the MTPA points. Between t =35s and t =70s, the proposed control has been trained and the convergence of the reference flux amplitude to the optimal is significantly quick. At t =70s, the rotor speed changes in step from 1000 r/min to 3000 r/min and the drive enters in the field weakening region. Under this condition, the self-learning control is suspended and $\mathbf{T}_{MTPA}$ and Ψ_{sMTPA} are not updated. The reference flux amplitude is directly limited by (6) and compensated by $\Delta\Psi_s$. The reference torque, the resultant torque and the reference flux amplitude are shown in Fig. 10. Since the maximum torque is limited by the peak torque profile in the field weakening region, thus the resultant torque is limited at 35 N·m between t = 95s and t = 105s when the speed is 3000 r/mim. At t=105 s, the speed decreases from 3000 r/min to 1000 r/min and the self-learning control is activated. The accurate reference flux amplitude is directly approximated by the SLC with almost no delay. It should be noted that the step changes in speed in the foregoing simulation are exaggerated to illustrate the robustness of the proposed control in response to rapid change of operating conditions between constant torque and field weakening regions. In reality, step change in speed is unlikely due to mechanical inertia and finite torque. It is also seen that the torque ripple increases significantly in the field weakening region. This is because the flux linkage in a real machine which is represented by the high fidelity model is a non-linear function of the currents and contains high order spatial harmonics as described in [25]. Consequently, the motor voltage is not sinusoidal and its interaction with the voltage limit gives rise to current distortion and hence significant increase in torque ripple at high speeds. The details of the cause of the large torque ripple are given in [25].
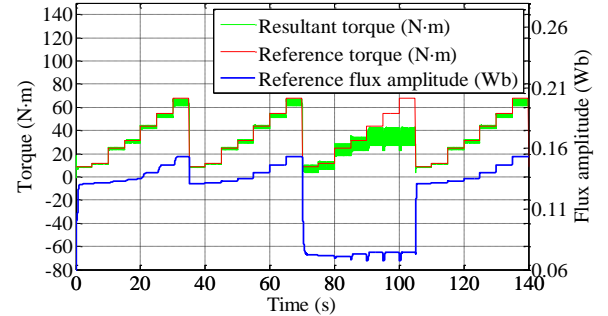

Fig. 10. Responses of reference torque and resultant torque when speed steps between 1000 r/min and 3000 r/min.

V. Experimental Result

The proposed self-learning control scheme has been tested on a prototype IPMSM drive. The IPMSM whose specifications are listed in Table I was mounted on the test-rig as shown in Fig. 11. The IPMSM was controlled in torque control mode and loaded by a dynamometer. The resultant torque was measured by a high precision torque transducer. The values of μ, ε, N and the initial values of $\mathbf{T}_{MTPA}$, Ψ_{sMTPA} in the experiments are the same as those used in simulations. The proposed self-learning control is implemented in a DSP-FPGA based controller shown in Fig. 11 with a sampling frequency of 8 kHz.
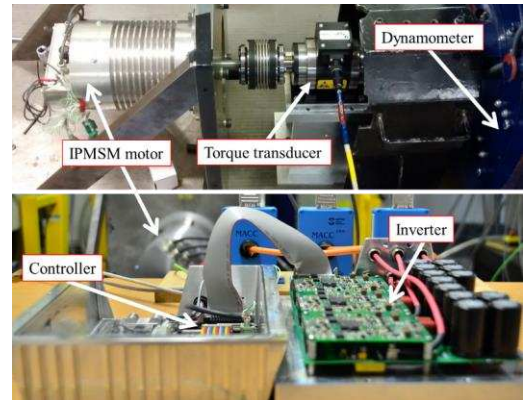

Fig. 11. IPMSM test-rig.

A. Self-learning Performance

The motor drive was first tested by increasing reference torque from 10 N·m to 35 N·m in steps of 5 N·m at 1000 r/min. During this period, the self-learning control scheme was trained. After the training, the reference torque decreased from 35 N·m to 10 N·m in steps of 5 N·m to verify the performance of the proposed self-learning control scheme. During this period, the SLC output, Ψ_{SLC}, of the proposed self-learning was generated from (14) based on data in Ψ_{sMTPA} and $\mathbf{T}_{MTPA}$ recorded in training.

Since the actual flux amplitude is difficult to measure, the measured d-axis current is utilized instead of flux amplitude to illustrate the self-learning performance of the proposed control

scheme. Fig. 12 illustrates the measured d-axis currents, the ideal MTPA d-axis currents, the measured torque when reference torque increases from 20 N·m to 35 N·m and decreases from 35 N·m to 20 N·m in steps of 5 N·m.

As shown in Fig. 12, when the reference torque steps from 20 N·m to 35 N·m when t <100 s, the proposed self-learning control has not been fully trained and Ψ_{SLC} is set to the flux amplitude associated with the maximum torque reference in $\mathbf{T}_{MTPA}$. The d-axis current slowly converges to the optimal d-axis current with the compensation of $\Delta\Psi_s$. However, after the proposed control scheme has been trained, i.e., when t >100s, the optimal reference flux amplitude is directly approximated by (14) and the small error of the approximation is compensated by $\Delta\Psi_s$ instantly. The speed of MTPA tracking response of the proposed control has been significantly increased. As a result, the d-axis current can reach the optimal value without much delay.
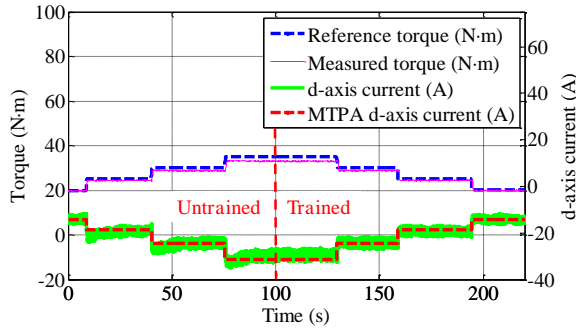

Fig. 12. Responses of resultant d-axis current and ideal MTPA d-axis current to reference torque changes.

The resultant MTPA quality indicator SPO and the resultant d-axis current under the same operation conditions of Fig. 12 are shown in Fig. 13. As can be seen from Fig. 13, before the proposed control scheme is trained, i.e., when t <100s, SPO is initially large after at each torque step and then converges to zero gradually. This is because of the large error between Ψ_{SLC} and the optimal flux amplitude as well as the slow convergence of $\Delta\Psi_s$ through the integral action. However, after the proposed control scheme has been trained, SPO converges to zero much fast. The improvement in the d-axis current response due to the proposed self-learning control scheme can be clearly seen in Fig. 13.
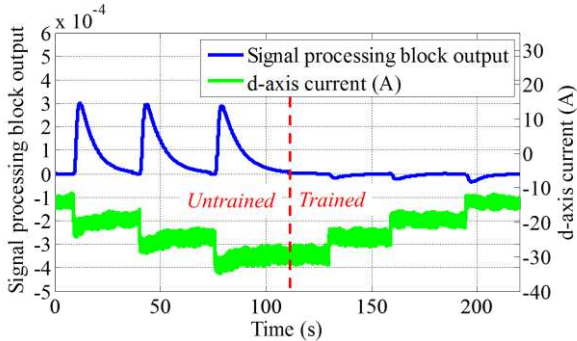

Fig. 13. MTPA quality indicator SPO and resultant d-axis current.

Fig. 14 shows the resultant d-axis current and reference torque when the torque command increases from 13 N·m to 18 N·m after the tests described previously. As shown in Fig. 14, the resultant d-axis current can track the ideal MTPA d-axis currents accurately with fast response even though the

proposed control scheme has not been trained at 18 N·m torque command previously.
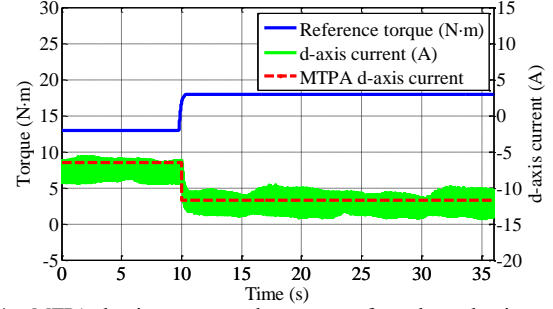

Fig. 14. MTPA d-axis current and response of resultant d-axis current to reference torque change from 13 N·m to 18 N·m.

The measured torque and reference torque under the same operation conditions as Fig. 14 are compared in Fig. 15. The reference torque is filtered by a low-pass filter to limit the rate of change of torque. The measured torque follows the reference torque well. Since the torque is generated based on (3), the dynamic response of torque depends on the bandwidth of the t-axis current control loop. Therefore, the torque response of the self-learning control should be the same as the torque response of the conventional direct flux vector control proposed in [7] and [22].
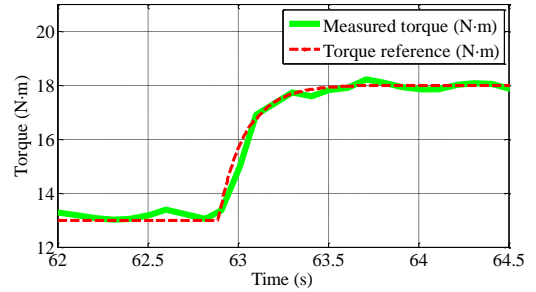

Fig. 15. Measured torque in response to reference torque change.

B. Transition Between Constant Torque Region and Field Weakening Region

Seamless transition from the constant torque region to field weakening region was also tested. In the field weakening region when v_{error} is smaller than the pre-defined threshold μ or $T_e^* \geq T_{lim}^*$, Ψ_{sMTPA} and $\mathbf{T}_{MTPA}$ updates will be suspended. Ψ_{SLC} is still generated from the data recorded in Ψ_{sMTPA} and $\mathbf{T}_{MTPA}$ according to (14), however, it will be limited by (6) in field weakening region.

Fig. 16 illustrates the transition from the field weakening region to the constant torque region when the reference torque is 20 N·m and the speed decreases from 1750 r/min to 1550 r/min. When speed is 1750 r/min, the motor is running in the field weakening. Under this condition, the reference flux amplitude, Ψ_{SLC}, generated from (14) is limited by (6). As the speed decreases, the resultant d-axis current increases (its magnitude in the negative d-axis direction decreases). When the motor speed reaches 1640 r/min, the stator flux amplitude or measured d-axis becomes a constant with further reduction in speed. This implies the transition from the field weakening operation to the constant torque region takes place at 1640 r/min and the smooth transition between field weakening region and constant torque region can be inferred. A similar test

was also performed when the motor speed was increased from the constant torque region to the field weakening region, and a smooth transition was also obtained.
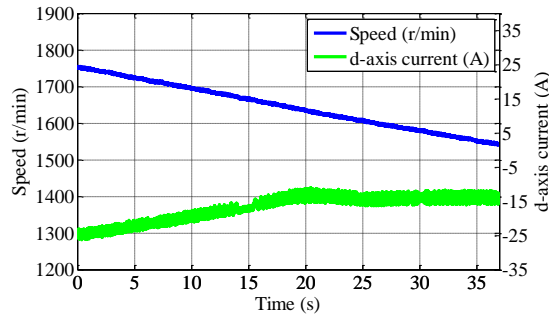

Fig. 16.   Speed and measured d-axis current during transition from field-weakening region to constant torque region.

C. Performance of Proposed Control Scheme in Deep Field Weakening Region

In the field weakening region, the fast dynamic response of the reference flux amplitude can be achieved by (6) directly instead of Ψ_{SLC}. The error of the reference flux amplitude due to inaccurately observed t- and f-axis currents or the inaccurate nominal stator resistance can be compensated by $\Delta\Psi_s$. Fig. 17 shows the maximum voltage amplitude, the reference voltage amplitude and the measured d-axis current when the reference torque steps from 20 N·m to 25 N·m at 3000 r/min (more than two times the base speed). A fast responses of d-axis current can be observed from Fig. 17. Moreover, the reference voltage amplitude is essentially equal to the maximum voltage amplitude, which means that the motor operation is kept at the VCMTPA point. The small error between the reference voltage amplitude and the maximum voltage amplitude is due to the combined effect of the inverter voltage drop and the virtual signal injection which always tends to drive the reference voltage amplitude to go beyond the maximum voltage.
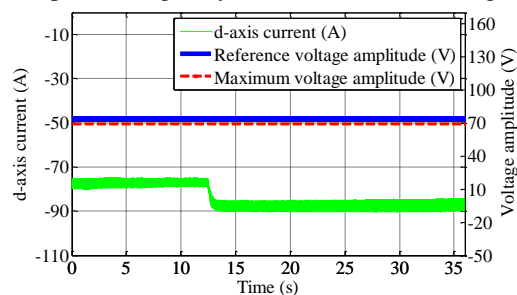

Fig. 17.   Maximum voltage amplitude, reference voltage amplitude and measured d-axis current when torque reference steps from 20 N·m to 25 N·m at 3000 r/min.

The comparison between the reference torque and the measured torque when the reference torque increased from 20 N·m to 25 N·m at 3000 r/min is shown in Fig. 18. The gap between the reference and measured torque is due to the flux observer inaccuracy and the frictional torque of the motor. The torque error can be mitigated by a more accurate flux observer or corrected by the speed feedback loop in a speed servo drive. For EV tractions, the feedback correction will be performed by a human driver.
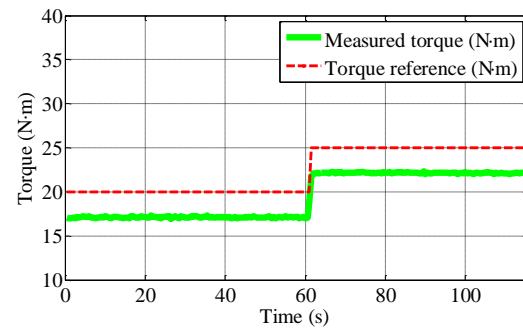

Fig. 18.   Comparison between reference torque and measured torque when reference torque increased from 20 N·m to 25 N·m at 3000 r/min.

VI.   CONCLUSION

A self-learning control for direct flux vector controlled IPMSM drives has been described. The online-learning is based on the virtual signal injection which tracks MTPA or VCMTPA points without prior knowledge of the machine parameters. It has been shown that after training, the proposed control generates optimal reference flux amplitudes for MTPA and VCMTPA control in constant torque and field weakening regions, respectively, without much delay. The proposed control scheme facilitates efficient operation of IPMSM drives and can adapt to machine parameter changes through self-learning. It has also been shown that the transition between the constant torque and field weakening operations is smooth and automatic. The performance of the proposed control scheme has been validated by simulations and experiments. The concept of the proposed self-learning control is also applicable to other search based optimal control schemes in the f-t reference frame to improve dynamic response.

REFERENCES

[1]   T. Miyajima, H. Fujimoto, and M. Fujitsuna, "A Precise Model-Based Design of Voltage Phase Controller for IPMSM," IEEE Trans. Power Electron., vol. 28, no. 12, pp. 5655–5664, Dec. 2013.

[2]   A. Ahmed, Y. Sozer, and M. Hamdan, "Maximum Torque per Ampere Control for Interior Permanent Magnet Motors using DC Link Power Measurement," IEEE Trans. Power Electron., in press, 2016.

[3]   M. Preindl and S. Bolognani, "Optimal State Reference Computation with Constrained MTPA Criterion for PM Motor Drives," IEEE Trans. Power Electron., vol. 30, no. 8, pp. 4524–4535, Aug. 2015.

[4]   E. Daryabeigi, H. Abootorabi Zarchi, G. R. Arab Markadeh, J. Soltani, and F. Blaabjerg, "Online MTPA Control Approach for Synchronous Reluctance Motor Drives Based on Emotional Controller," IEEE Trans. Power Electron., vol. 30, no. 4, pp. 2157–2166, Apr. 2015.

[5]   T. Sun and J. Wang, "Extension of Virtual Signal Injection Based MTPA Control for Interior Permanent Magnet Synchronous Machine Drives into Field Weakening Region," IEEE Trans. Ind. Electron., vol. 62, no. 11, pp. 6809–6817, Nov. 2015.

[6]   T. Sun, J. Wang, and X. Chen, "Maximum Torque per Ampere (MTPA) Control for Interior Permanent Magnet Synchronous Machine Drives Based on Virtual Signal Injection," IEEE Trans. Power Electron., vol. 30, no. 9, pp. 5036–5045, Sept. 2015.

[7]   G. Pellegrino, E. Armando, and P. Guglielmi, "Direct-Flux Vector Control of IPM Motor Drives in the Maximum Torque Per Voltage Speed Range," IEEE Trans. Ind. Electron., vol. 59, no. 10, pp. 3780–3788, Oct. 2012.

[8]   L. Tang, L. Zhong, M. F. Rahman, and Y. Hu, "A Novel Direct Torque Controlled Interior Permanent Magnet Synchronous Machine Drive With Low Ripple in Flux and Torque and Fixed Switching Frequency," IEEE Trans. Power Electron., vol. 19, no. 2, pp. 346–354, Mar. 2004.

[9]   Y.-S. Choi, H. H. Choi, and J.-W. Jung, "Feedback Linearization Direct Torque Control with Reduced Torque and Flux Ripples for IPMSM

Drives," IEEE Trans. Power Electron., vol. 31, no. 5, pp. 3728–3737, May. 2016.

[10] M. Koc, J. Wang, and T. Sun, "An Inverter Nonlinearity Independent Flux Observer for Direct Torque Controlled High Performance Interior Permanent Magnet Brushless AC Drives," IEEE Trans. Power Electron., vol. in press, 2016.

[11] C. Xia, J. Zhao, Y. Yan, and T. Shi, "A Novel Direct Torque Control of Matrix Converter-Fed PMSM Drives Using Duty Cycle Control for Torque Ripple Reduction," IEEE Trans. Ind. Electron., vol. 61, no. 6, pp. 2700–2713, Jun. 2014.

[12] T. Inoue, Y. Inoue, S. Morimoto, and M. Sanada, "Mathematical Model for MTPA Control of Permanent-Magnet Synchronous Motor in Stator Flux Linkage Synchronous Frame," IEEE Trans. Ind. Appl., vol. 51, no. 5, pp. 3620–3628, Sept.-Oct. 2015.

[13] S.-Y. Jung, J. Hong, and K. Nam, "Current Minimizing Torque Control of the IPMSM Using Ferrari's Method," IEEE Trans. Power Electron., vol. 28, no. 12, pp. 5603–5617, Dec. 2013.

[14] T. Sun, J. Wang, and M. Koc, "Virtual Signal Injection Based Direct Flux Vector Control of IPMSM Drives," IEEE Trans. Ind. Electron., vol. 63, no. 8, pp. 4773 – 4782, Aug. 2016.

[15] A. Shinohara, Y. Inoue, S. Morimoto, and M. Sanada, "Correction of Reference Flux for MTPA Control in Direct Torque Controlled Interior Permanent Magnet Synchronous Motor Drives," in Proc. IEEE IPEC., 2014, pp. 324–329.

[16] S. Bolognani, L. Peretti, and M. Zigliotto, "Online MTPA Control Strategy for DTC Synchronous-Reluctance-Motor Drives," IEEE Trans. Power Electron., vol. 26, no. 1, pp. 20–28, Jan. 2011.

[17] Y. Tan, W. H. Moase, C. Manzie, D. Nešić, and I. M. Y. Mareels, "Extremum Seeking From 1922 To 2010," in Proc. IEEE CCC, 2010, pp. 14–26.

[18] R. Antonello, M. Carraro, and M. Zigliotto, "Maximum-Torque-Per-Ampere Operation of Anisotropic Synchronous Permanent-Magnet Motors Based on Extremum Seeking Control," IEEE Trans. Ind. Electron., vol. 61, no. 9, pp. 5086–5093, Sep. 2014.

[19] S. Kim, Y.-D. Yoon, S.-K. Sul, and K. Ide, "Maximum Torque per Ampere (MTPA) Control of an IPM Machine Based on Signal Injection Considering Inductance Saturation," IEEE Trans. Power Electron., vol. 28, no. 1, pp. 488–497, Jan. 2013.

[20] S. Bolognani, R. Petrella, A. Prearo, and L. Sgarbossa, "Automatic Tracking of MTPA Trajectory in IPM Motor Drives Based on AC Current Injection," IEEE Trans. Ind. Appl., vol. 47, no. 1, pp. 105–114, Jan. 2011.

[21] T. Sun, J. Wang, M. Koc, and X. Chen, "Self-Learning MTPA Control of Interior Permanent Magnet Synchronous Machine Drives Based on Virtual Signal Injection," IEEE Trans. Ind. Appl., vol. 52, no. 4, pp. 3062 – 3070, July-Aug. 2016.

[22] G. Pellegrino, E. Armando, and P. Guglielmi, "Direct Flux Field-Oriented Control of IPM Drives With Variable DC Link in the Field-Weakening Region," IEEE Trans. Ind. Appl., vol. 45, no. 5, pp. 1619–1627, Sept.-Oct. 2009.

[23] G. Pellegrino, R. I. Bojoi, and P. Guglielmi, "Unified Direct-Flux Vector Control for AC Motor Drives," IEEE Trans. Ind. Appl., vol. 47, no. 5, pp. 2093–2102, Sept.-Oct. 2011.

[24] A. Yoo and S.-K. Sul, "Design of Flux Observer Robust to Interior Permanent-Magent Synchronous Motor Flux Variation," IEEE Trans. Ind. Appl., vol. 45, no. 5, pp. 1670–1677, Sept.-Oct.2009.

[25] X. Chen, J. Wang, B. Sen, P. Lazari, and T. Sun, "A High-Fidelity, Computationally Efficient Model for Interior Permanent Magnet Machines Considering the Magnetic Saturation, Spatial Harmonics and Iron Loss Effect," IEEE Trans. Ind. Electron., vol. 62, no. 7, pp. 4044–4055, Jul. 2015.

Tianfu Sun (S'15) was born in China. He received B.Eng. degree in mechanical engineering, M.Sc. degree in civil engineering from Dalian University of Technology, Dalian, China, in 2009 and 2012, respectively and the Ph.D. degree in electrical and electronic engineering from the University of Sheffield, Sheffield, U.K., in 2016.

He is currently working as a research associate in electric drives at The University of Sheffield, U.K. His current research interests include electric/hybrid vehicle drives, power-electronic control of electric machines, thermal management and artificial intelligence.

Jiabin Wang (SM'03) received the B.Eng. and M.Eng. degrees from Jiangsu University of Science and Technology, Zhenjiang, China, in 1982 and 1986, respectively, and the Ph.D. degree from the University of East London, London, U.K., in 1996, all in electrical and electronic engineering.

Currently, he is a Professor in Electrical Engineering at the University of Sheffield, Sheffield, U.K. From 1986 to 1991, he was with the Department of Electrical Engineering at Jiangsu University of Science and Technology, where he was appointed a Lecturer in 1987 and an Associated Professor in 1990. He was a Postdoctoral Research Associate at the University of Sheffield, Sheffield, U.K., from 1996 to 1997, and a Senior Lecturer at the University of East London from 1998 to 2001. His research interests range from motion control and electromechanical energy conversion to electric drives for applications in automotive, renewable energy, household appliances and aerospace sectors.

He is a fellow of the IET and a senior member of IEEE.

Mikail Koc (S'15) was born in Turkey. He received the BSc degree from ESOGU University, Eskisehir, Turkey, in 2009 and the MSc degree from Nottingham University, UK, in 2012 both in electrical and electronic engineering. He is currently pursuing the PhD degree in electronic and electrical engineering at the University of Sheffield, UK. His research interests include efficiency optimised control of motors for electric vehicle traction.